Iontronic Neuromorphic Signaling with Conical Microfluidic Memristors

T. M. Kamsma,[1,2] W. Q. Boon,[1] T. ter Rele,[1,3] C. Spitoni,[2] and R. van Roij[1]
[1]Institute for Theoretical Physics, Utrecht University, Princetonplein 5, 3584 CC Utrecht, Netherlands
[2]Mathematical Institute, Utrecht University, Budapestlaan 6, 3584 CD Utrecht, Netherlands
[3]Soft Condensed Matter, Debye Institute for Nanomaterials Science, Utrecht University, Princetonplein 1, 3584 CC Utrecht, Netherlands

(Received 22 December 2022; accepted 25 May 2023; published 26 June 2023)

Experiments have shown that the conductance of conical channels, filled with an aqueous electrolyte, can strongly depend on the history of the applied voltage. These channels hence have a memory and are promising elements in brain-inspired (iontronic) circuits. We show here that the memory of such channels stems from transient concentration polarization over the ionic diffusion time. We derive an analytic approximation for these dynamics which shows good agreement with full finite-element calculations. Using our analytic approximation, we propose an experimentally realizable Hodgkin-Huxley iontronic circuit where micrometer cones take on the role of sodium and potassium channels. Our proposed circuit exhibits key features of neuronal communication such as all-or-none action potentials upon a pulse stimulus and a spike train upon a sustained stimulus.

DOI: 10.1103/PhysRevLett.130.268401

Transport phenomena of charged species through channels in the nanometer and micrometer regime play a key role in a plethora of applications [1–12]. An exciting emerging direction of research is that of iontronics, the use of ion transport for signaling [13], which holds the promise of interfacing with biological systems [13–16] and processing information via multiple signal carriers and chemical regulation [17,18]. In particular, conical channels have garnered significant interest for such applications [14,15,19–23], as they exhibit current rectification thereby acting as ionic diodes [9,19,24–26]. This has been extensively studied experimentally [19,22,27–31] as well as numerically [23,32–35] and several analytic descriptions are available [25,36–38]. Because of this interest cones are now comparatively easy to fabricate [39–42]. Recently, it has been observed that the conductance of cones exhibits hysteresis when driven by an alternating potential [43–53], and hence they are memristors (resistors with memory) [54–57]. Various explanations of this effect have been explored [43–48], the most recent hypothesis being dynamic concentration polarization [50–53], which we confirm below. Memristors in general are essential components for neuromorphic (brain-inspired) circuits, since much of their dynamics is analogous to the synapses that connect neurons [58–62] and to the ion channels responsible for electric signaling within neurons [58,63]. The popularity of memristors and neuromorphic circuits has drastically increased [64–66] due to the prospects of energy-efficient computers [67–69] and biocompatibility [59,70–74]. Solid-state devices received the majority of attention [64–66,68], while the brain in contrast relies on ion transport in an aqueous medium [75,76]. Iontronic circuits, based on the same signaling medium as the brain, sparked recent interest as a promising platform for a new generation of (neuromorphic) computing devices [17,77–80]. However, the development of neuromorphic iontronic devices is still in its infancy [13,79] and a deeper understanding of underlying mechanisms and possible end uses is needed [79,80].

In this Letter we propose a neuromorphic iontronic circuit where all-or-none action potentials (APs) [75,76,81] and neuronal spiking [76,82–85] are obtained through micrometer cones filled with aqueous electrolyte. First we solve for the dynamic competition between ionic diffusion, conduction, and advection, using the Poisson-Nernst-Planck-Stokes (PNPS) equations and the steady-state results in Ref. [25]. We obtain a differential equation with no free parameters describing transient concentration polarization and we surprisingly find that the inhomogeneous conduction responsible for concentration polarization retains memory over slow (diffusive) timescales. Using this result we construct an experimentally accessible iontronic circuit of several cones, batteries, and a capacitor and show that the time-dependent voltage over this circuit exhibits multiple key features of neuronal communication. While neuronal behavior in the form of an emerging voltage spike train has been reported in a simulated iontronic circuit containing quasi-two-dimensional nanochannels that connect aqueous electrolytes [86], the defining all-or-none law of action potentials [75,76,81], a phenomenon considered to be a requirement for artificial neurons [66], has not yet been reported. Furthermore, the circuit in Ref. [86] requires comparatively difficult to fabricate two-dimensional channels and Nernst potentials

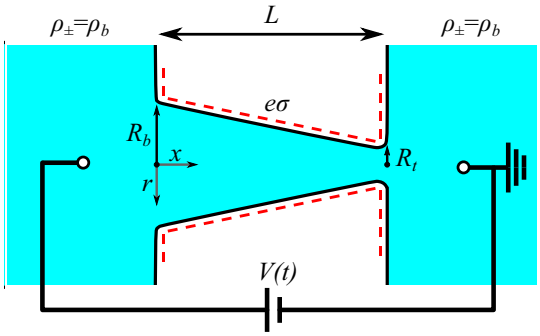

FIG. 1. Schematic representation of an azimuthally symmetric conical channel of length L, base radius R_b, and tip radius $R_t < R_b$, connecting two bulk reservoirs of a 1:1 aqueous electrolyte, with bulk concentrations ρ_b. The channel wall carries a surface charge density $e\sigma$. An ac electric potential drop $V(t)$ over the channel drives an ionic charge current $I[V(t),t] = g[V(t),t]V(t)$, with $g[V(t),t]$ the channel conductance. The ac potential causes transient concentration polarization resulting in a volatile conductance memory.

that do not directly affect the circuit voltage, complicating experimental accessibility. In this Letter we overcome these issues. As conical pores are a well-known iontronic model system, we believe our proposed neuromorphic circuit is within experimental reach.

We first consider a single conical channel, schematically illustrated in Fig. 1, that connects two bulk reservoirs of an incompressible aqueous 1:1 electrolyte at temperature $T = 293.15$ K, with viscosity $\eta = 1.01$ mPa s, mass density $\rho_m = 10^3$ kg m^{-3}, and electric permittivity $\varepsilon = 0.71$ nF m^{-1}, containing ions with diffusion coefficients $D_\pm = D = 1.75$ μm^2 ms^{-1} and charge $\pm e$ with e the proton charge. At the far side of both reservoirs we impose a fixed pressure $P = P_0$ and fixed ion concentrations $\rho_\pm = \rho_b = 0.1$ mM. The reservoirs are connected by an azimuthally symmetric conical channel with base radius $R_b = 200$ nm at $x = 0$ and tip radius $R_t = R_b - \Delta R = 50$ nm at $x = L \gg R_b$, the central axis being at radial coordinate $r = 0$. Unless otherwise stated the channel has length $L = 10$ μm; hence the geometry is similar to cones in Ref. [39]. The channel radius is described by $R(x) = R_b - x\Delta R/L$ for $x \in [0, L]$. We assume a uniform surface charge density $e\sigma = -0.0015e$ nm^{-2} on the channel walls, resulting in a surface potential $\psi_0 \approx -10$ mV (typical for PMMA [87]) and an electric double layer that screens the surface charge with Debye length $\lambda_D \approx 30$ nm. On the far side of the reservoir connected to the base we impose an electric potential $V(t)$, while the far side of the other reservoir is grounded, which leads to an electric potential profile $\Psi(x,r,t)$, an electro-osmotic fluid flow with velocity field $\mathbf{u}(x,r,t)$, and ionic fluxes $\mathbf{j}_\pm(x,r,t)$ with $\mathbf{j}_+ - \mathbf{j}_-$ the charge flux. A relatively low surface potential ψ_0 ensures a weak electro-osmotic flow $Q(V)$, allowing conductance tuning over a wider voltage range [25,49,88]. We have $Q(V)/V = -\pi R_t R_b \varepsilon\psi_0/(\eta L) \approx 22.7$ μm^3 s^{-1} V^{-1} for our standard parameter set [25].

Transport through the conical channel is described by the Poisson-Nernst-Planck-Stokes equations (1)–(4) given by

$$\nabla^2\Psi = -\frac{e}{\varepsilon}(\rho_+ - \rho_-), \tag{1}$$

$$\frac{\partial\rho_\pm}{\partial t} + \nabla\cdot\mathbf{j}_\pm = 0, \tag{2}$$

$$\mathbf{j}_\pm = -D_\pm\left(\nabla\rho_\pm \pm \rho_\pm\frac{e\nabla\Psi}{k_BT}\right) + \mathbf{u}\rho_\pm, \tag{3}$$

$$\rho_m\frac{\partial\mathbf{u}}{\partial t} = \eta\nabla^2\mathbf{u} - \nabla P - e(\rho_+ - \rho_-)\nabla\Psi, \qquad \nabla\cdot\mathbf{u} = 0. \tag{4}$$

Here electrostatics is accounted for by the Poisson Eq. (1), the conservation of ions by the continuity Eq. (2), the combination of Fickian diffusion, Ohmic conduction, and Stokesian advection by the Nernst-Planck Eq. (3), and finally the force balance on the (incompressible) fluid by the Stokes Eq. (4). This system is closed upon imposing no-slip and blocking boundary conditions on the channel wall, $\mathbf{u} = 0$ and $\mathbf{n}\cdot\mathbf{j}_\pm = 0$, respectively, together with Gauss's law $\mathbf{n}\cdot\nabla\Psi = -e\sigma/\varepsilon$, with $\mathbf{n}$ the wall's inward normal vector.

When an electric potential $V(t)$ is applied, the ionic concentrations $\rho_\pm(x,r,t)$ will deviate from their equilibrium profiles, thereby changing the channel conductance [25]. In Ref. [25] the stationary state version of the PNPS equations (1)–(4) is solved for a static potential V, which gives rise to the stationary charge current $I = g_\infty(V)V$, where the static conductivity $g_\infty(V)$ was found to be governed by the (voltage-dependent) radially averaged salt concentration $\bar\rho_s(x,V) = 2\int_0^{R(x)} r\rho_s(x,V,r)dr/R(x)^2$, with $\rho_s = \rho_+ + \rho_-$ [see Supplemental Material (SM) for full expression [89]]. For small potentials $e|V|/k_BT \ll |w|(R_b/R_t)$, with $w = eD\eta/(k_BT\varepsilon\psi_0) \simeq -9.5$ the ratio of ionic to electro-osmotic mobility [88], the pore concentration equals the bulk concentration $\bar\rho_s(x,V) = 2\rho_b$, yielding $g_\infty(V) = g_0$, with the Ohmic cone conductance $g_0 = (\pi R_t R_b/L)(2\rho_b e^2 D/k_BT)$, and the resulting current follows Ohm's law $I = g_0 V$ [25]. For large static potential drops the cone exhibits diodic behavior due to concentration polarization, with the cone conductance determined by the salt concentration profiles according to

$$\frac{g_\infty(V)}{g_0} = \int_0^L \bar\rho_s(x,V)dx/(2\rho_b L) = 1 + \Delta g\int_0^L\left[\frac{x}{L}\frac{R_t}{R(x)} - \frac{e^{\mathrm{Pe}(V)(x/L)[R_t^2/R_bR(x)]} - 1}{e^{\mathrm{Pe}(V)(R_t/R_b)} - 1}\right]dx/L, \tag{5}$$

where an approximation is made compared to the more accurate dependence on $L/\int_0^L[\bar{\rho}_s(x,V)]^{-1}dx$ to reduce computational complexity [25]. The static conductance $g_\infty(V)$ depends on V through the Péclet number at the narrow end $\mathrm{Pe}(V) = Q(V)L/(D\pi R_t^2) = -(eV/k_BT)(R_b/R_t)w^{-1}$, where for our standard parameters $\mathrm{Pe}(V)/V \approx 16.5\ \mathrm{V}^{-1}$, and $\Delta g \equiv -2w(\Delta R/R_b)\mathrm{Du} \approx -3.6$ with the tip Dukhin number $\mathrm{Du} = \sigma/(2\rho_b R_t) \approx -0.25$. In our case of $\sigma < 0$, $V > 0$ depletes the channel of ions such that $g_\infty(V)/g_0 < 1$, whereas $V < 0$ results in ion accumulation such that $g_\infty(V)/g_0 > 1$, which is responsible for the static diode behavior of the cone [25].

Voltage-driven accumulation or depletion of ions from the pore is not instantaneous, as it takes time for the ions to move into or out of the channel. In the SM [89] we derive from the PNPS equations (1)–(4) that the typical timescale for this process is not given by an RC-like time as suggested in Ref. [46], but rather by a diffusionlike time,

$$\tau = \frac{L^2}{12D}, \tag{6}$$

which for our standard parameter set yields $\tau = 4.8$ ms. To obtain an analytic approximation for the time-dependent conductance $g[V(t),t]$, we assume a single exponential relaxation of the salt concentration with timescale τ toward the steady-state concentration profile. This natural approach has been successfully applied to investigate memristor dynamics before [78,97] and is verified for conical channels in Fig. 2. Using Eq. (5), this approach yields the following expressions for the time-dependent conductance $g[V(t),t]$ and current $I[V(t),t]$:

$$\frac{\partial g[V(t),t]}{\partial t} = \frac{g_\infty[V(t)] - g[V(t),t]}{\tau}, \tag{7}$$

$$I[V(t),t] = g[V(t),t]V(t). \tag{8}$$

Equation (7) shows that the conductance $g[V(t),t]$ depends on the entire time trace of the potential $V(t)$. This conductance memory is the key feature of a memristor [57]; in fact, Eqs. (7) and (8) indeed fit the mathematical definition of a generic voltage-driven memristor [56–58]. From now on we will refer to Eqs. (5)–(8) as the approximate analytical (AA) solution of the PNPS equations [25]. To verify the AA we also numerically solve the full PNPS equations (1)–(4) in the geometry of a conical channel using the finite-element (FE) analysis package COMSOL [98,99].

In Fig. 2(a) we compare the time-dependent laterally averaged salt concentrations $\langle\bar{\rho}_s\rangle[V(t),t] \equiv \int_0^L \bar{\rho}_s[x,V(t),t]dx/L$ from FE calculations (blue line) and the AA (red line), which for the AA is equivalent to $g[V(t),t]/g_0$. In both cases $V(t)$ is a periodic triangle potential (green line) with amplitudes ± 1 V and a period of 25 ms. The features of the AA and FE calculations essentially agree, not only the typical amplitude of $\langle\bar{\rho}_s\rangle[V(t),t]$, but also the time lag $\sim\tau$ [Eq. (6)] between $V(t)$ and $\langle\bar{\rho}_s\rangle[V(t),t]$, as indicated by the two pairs of dashed vertical lines. This time lag results in a hysteretic conductance-voltage diagram, shown in Fig. 2(b). Here the AA and FE calculations agree with each other again, verifying the proposed relation of $\langle\bar{\rho}_s\rangle[V(t),t]$ with the conductance $g[V(t),t]$.

Translating the results of Fig. 2(b) to the current with Eq. (8) we obtain the current-voltage (I-V) plot of Fig. 2(c), which shows the memristor hallmark of a pinched hysteresis loop [56]. We again find agreement between the AA and FE calculations, and the I-V loop resembles previously reported experimental results from comparable systems [43–45,49,52]. The shape of the hysteresis loop depends on the frequency f of the applied triangle potential

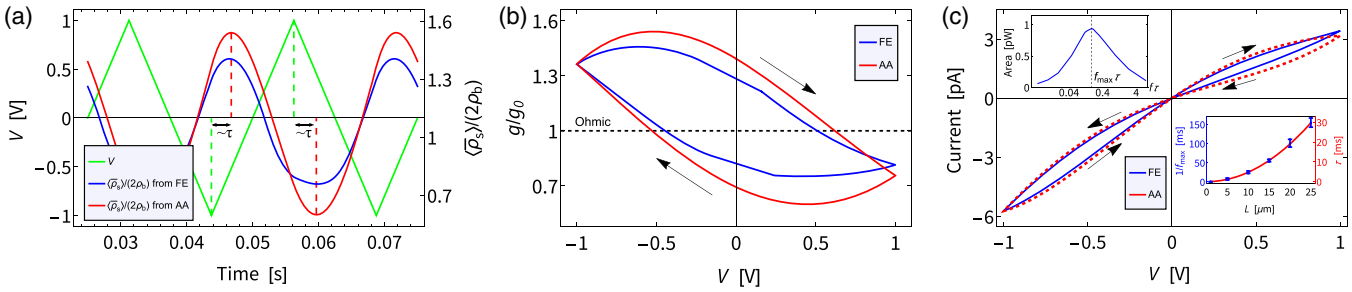

FIG. 2. Comparisons of finite-element (FE) calculations (blue) of the full PNPS equations (1)–(4) and our analytic approximation (AA) Eqs. (5)–(8) (red) when a periodic triangle potential $V(t)$ [green line in (a)] with amplitudes ± 1 V and frequency $f = 40$ Hz is applied. In (a) we show two periods of the time-dependent laterally averaged salt concentration $\langle\bar{\rho}_s\rangle[V(t),t] \equiv \int_0^L \bar{\rho}_s[x,V(t),t]dx/L$, in (b) the corresponding conductance-voltage diagram as per Eqs. (5) and (7), and in (c) the corresponding current-voltage diagram with a clear pinched hysteresis loop. The left-hand inset of (c) shows the dependence of the enclosed area in I-V hysteresis loop on the (dimensionless) triangle potential frequency $f\tau$ with a maximum at $f_{\max}\tau \approx 0.19$ for $L = 10$ μm. The right-hand inset of (c) shows the dependence of $1/f_{\max}$ (blue) and of the characteristic time τ from Eq. (6) (red) on the channel length L, satisfying $f_{\max}\tau \approx 0.19$ for all L considered.

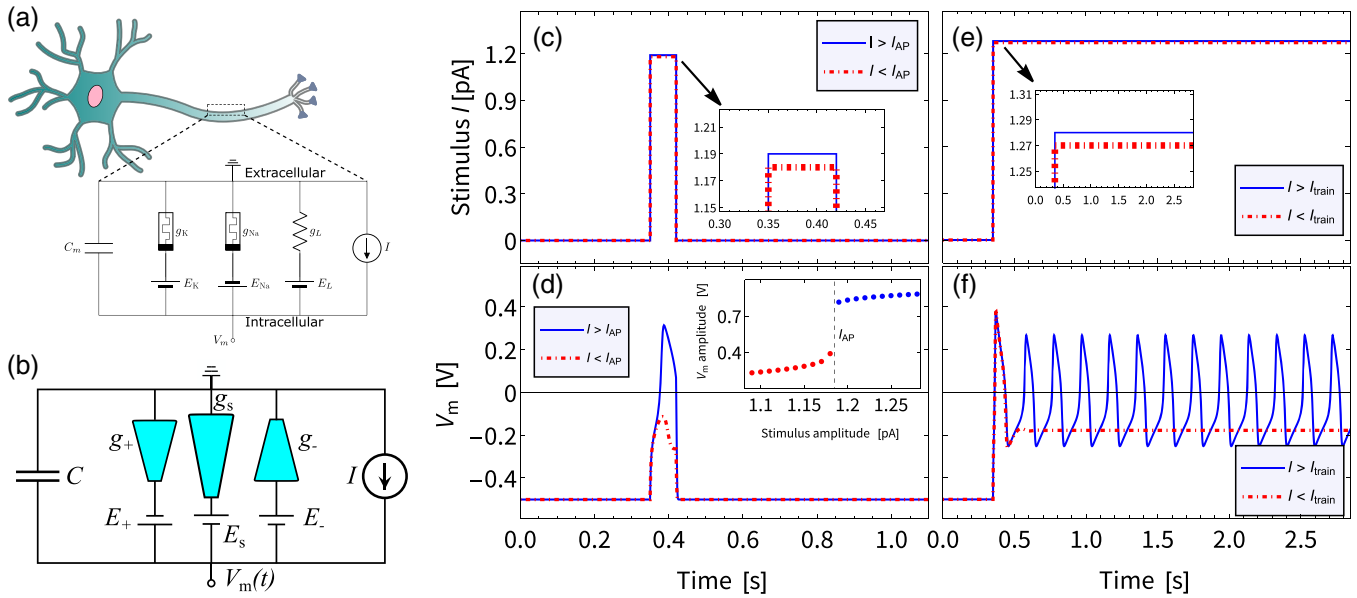

FIG. 3. (a) The Hodgkin-Huxley circuit model with Na^+, K^+, and leak channels, a capacitor and batteries corresponding to the Na^+ and K^+ Nernst potentials [100]. (b) Schematic representation of our proposed circuit containing three oriented conical channels, connected in series to individual batteries and in parallel to a capacitor. The electric potential difference $V_m(t)$ over the capacitor can be driven by an imposed stimulus current $I(t)$. (c) The imposed subcritical (red) and supercritical (blue) current pulse $I(t)$, and (d) the resulting $V_m(t)$ from Eq. (9), displaying an all-or-none action potential, as can be seen by the jump in spike amplitude around I_{AP} as shown in the inset. (e) The imposed subcritical (red) and supercritical (blue) sustained currents $I(t)$, and (f) the resulting $V_m(t)$, where a spike train emerges for $I(t) > I_{train}$.

$V(t)$. The enclosed area inside the loop shrinks to 0 for $f\tau \ll 1$ and $f\tau \gg 1$ and shows a maximum at $f_{max}\tau \approx 0.19$ for the standard parameter set, as shown in the left-hand inset of Fig. 2(c). In the right-hand inset of Fig. 2(c) we see that the one-to-one relation $f_{max}\tau \approx 0.19$ also holds for various lengths L, further supporting the validity of Eq. (6). Excitingly, the quadratic dependence of τ on the channel length L offers strong control over the channel memory retention time, a desirable trait [61].

Having derived Eqs. (6)–(8) for the memristive effect in a single conical channel, we now turn our attention to modeling a brain-inspired iontronic circuit. Electric signaling within a neuron is facilitated by an action potential, a propagating voltage spike over the cell membrane [75]. APs obey the all-or-none law, i.e., an AP either fails to initiate upon a subcritical stimulus or completely occurs for a supercritical stimulus, with no gradual transition in between [75,76,81], and can be sequentially generated, resulting in a spike train [76,82–85]. These neuronal features of electric activity over the membrane have been successfully modeled by an equivalent circuit as in Fig. 3(a), first quantitatively characterized by Hodgkin and Huxley [100], which has formed an extensively used basis to mathematically model neuronal signaling [101–107]. Interestingly, the mathematical descriptions of the biological potassium and sodium channel conductances g_K and g_{Na} in the Hodgkin-Huxley (HH) model were later identified to be descriptions of memristors [63]. Therefore we expect similar spontaneous neuronal features by assembling conical channels in a HH-like circuit, where the micrometer channels take on the role of the potassium and sodium channels.

Inspired by HH circuits we present the circuit shown in Fig. 3(b). This circuit consists of a capacitor with capacitance $C = 5$ fF (corresponding to the typical capacitance of a biological neuronal membrane of area $\sim 1\ \mu m^2$ [108]), connected in parallel with three oriented conical channels, with conductances g_+, g_-, and g_s and lengths $L_\pm = 1$ μm and $L_s = 25$ μm. As per Eq. (6), the timescales $\tau_\pm \approx 0.048$ ms of the two fast channels are identical, while the timescale $\tau_s \approx 30$ ms $\gg \tau_\pm$ is much slower. The conical channels are connected in series to batteries with potentials $E_\pm = \pm 0.975$ V for the two fast channels and $E_s = -0.5$ V for the slow channel. The imposed stimulus current $I(t)$ is the control parameter and determines whether spiking occurs. The electric potential $V_m(t)$ over the circuit shown in Fig. 3(b) is equivalent to the membrane potential over a neuronal membrane [100]. Invoking Kirchoff's law, the potential $V_m(t)$ will evolve according to

$$C\frac{dV_m(t)}{dt} = I(t) - \sum_{i\in\{+,-,s\}} g_i[V_i(t),t][V_m(t) - E_i], \qquad (9)$$

where the conductances $g_i[V_i(t),t]$, determined by their individual laterally averaged salt concentrations as per Eq. (5), each evolve according to Eq. (7), however with

arguments V_i of $g_{i,\infty}(V_i)$ given by $V_-(t) = V_m(t) - E_-$, $V_+(t) = -V_m(t) + E_+$, and $V_s(t) = -V_m(t) + E_s$. The differences in signs of the potentials reflect the different orientations of the channels as depicted in Fig. 3(b). Equations (6), (7), and (9) form a closed set of equations, which we numerically solve with initial conditions $V(0) = -0.5$ V and $g_i[V_i(0), 0] = g_{0,i}$.

Figure 3(c) shows a subcritical pulse current $I < I_{\mathrm{AP}}$ (red) and supercritical pulse current $I > I_{\mathrm{AP}}$ (blue), both of duration 70 ms, and Fig. 3(d) shows the two resulting membrane potentials $V_m(t)$. For the supercritical stimulus $V_m(t)$ fully depolarizes and an AP emerges, while it fails to properly depolarize for the subcritical stimulus. The inset of Fig. 3(d) shows that the amplitude of the voltage spike undergoes a sharp step increase at the pulse strength $I = I_{\mathrm{AP}}$; i.e., the circuit exhibits the defining all-or-none law found in biological neurons [75,76,81], a feature considered to be a requirement for artificial neurons [66].

For a slightly increased and sustained stimulus strength [as shown in Fig. 3(e)], the spike train of Fig. 3(f) emerges for a supercritical input $I > I_{\mathrm{train}}$, while just a single AP appears for a subcritical input $I < I_{\mathrm{train}}$. Spike trains are another unique feature of neuromorphic behavior and play a vital role in neuronal communication [76,82–85]. In the SM [89] we show that the frequency of the spike train can be tuned by altering the capacitance and cone lengths. In Ref. [86] a spike train emerging from a simulated iontronic circuit containing quasi-two-dimensional nanochannels was presented. However, the defining all-or-none law of APs [66,75,76,81] was not reported in Ref. [86]. Additionally, in biological neurons the battery potentials stem from Nernst potentials, which are not considered to affect the voltage-gated channel conductances; hence $|V_i| = |V_m|$ in typical HH studies [100–107]. However, in an experimental realization of a microfluidic HH-like circuit with electric batteries the voltages $V_i(t)$ over the channels will be affected by the battery potentials E_i; i.e., $|V_i(t)| = |V_m(t) - E_i|$. This detail is not considered in Ref. [86] and hence it is not immediately clear how this circuit could be experimentally realized.

In summary, we derived a theoretical model with no free parameters, starting from the Poisson-Nernst-Planck-Stokes equations (1)–(4), that explains how dynamic concentration polarization in conical pores facilitates a volatile conductance memory. Our theory agrees quantitatively with the memristive conductance of conical channels observed in finite-element calculations and we surprisingly find that the conductive memory retention process is governed by a slow diffusive timescale. By assembling multiple conical channels in an experimentally accessible iontronic HH circuit, we find emerging neuronal behavior. The circuit exhibits all-or-none action potentials upon pulse stimulation, a fundamental requirement for artificial neurons [66], and spike trains under a sustained stimulus, thereby displaying hallmark features of neuronal communication [76,81–85]. Our work promises to accelerate the targeted development of iontronic circuits and a more effortless scanning of possible applications thereof, beyond what is presented in this Letter.

This work is part of the D-ITP consortium, a program of the Netherlands Organisation for Scientific Research (NWO) that is funded by the Dutch Ministry of Education, Culture and Science (OCW). T. M. K. performed the calculations, W. Q. B. conceptualized the work, T. M. K. and W. Q. B. developed the theory under supervision of C. S. and R. v. R. All authors discussed the results and contributed to the Letter.

[1] K. N. Knust, D. Hlushkou, U. Tallarek, and R. M. Crooks, ChemElectroChem **1**, 850 (2014).
[2] S. P. Surwade, S. N. Smirnov, I. V. Vlassiouk, R. R. Unocic, G. M. Veith, S. Dai, and S. M. Mahurin, Nat. Nanotechnol. **10**, 459 (2015).
[3] C.-C. Lai, C.-J. Chang, Y.-S. Huang, W.-C. Chang, F.-G. Tseng, and Y.-L. Chueh, Nano Energy **12**, 394 (2015).
[4] F. H. van der Heyden, D. J. Bonthuis, D. Stein, C. Meyer, and C. Dekker, Nano Lett. **7**, 1022 (2007).
[5] A. Siria, P. Poncharal, A.-L. Biance, R. Fulcrand, X. Blase, S. T. Purcell, and L. Bocquet, Nature (London) **494**, 455 (2013).
[6] K. Xiao, L. Jiang, and M. Antonietti, Joule **3**, 2364 (2019).
[7] O. A. Saleh and L. L. Sohn, Nano Lett. **3**, 37 (2003).
[8] W. Shi, A. K. Friedman, and L. A. Baker, Anal. Chem. **89**, 157 (2017).
[9] I. Vlassiouk, T. R. Kozel, and Z. S. Siwy, J. Am. Chem. Soc. **131**, 8211 (2009).
[10] A. De La Escosura-Muñiz and A. Merkoçi, ACS Nano **6**, 7556 (2012).
[11] H. Zhang, Y. Tian, and L. Jiang, Nano Today **11**, 61 (2016).
[12] Z. S. Siwy, M. L. Bruening, and S. Howorka, Chem. Soc. Rev. **52**, 1983 (2023).
[13] S. H. Han, M.-A. Oh, and T. D. Chung, Chem. Phys. Rev. **3**, 031302 (2022).
[14] C. Yang, K. Hu, D. Wang, Y. Zubi, S. T. Lee, P. Puthongkham, M. V. Mirkin, and B. J. Venton, Anal. Chem. **91**, 4618 (2019).
[15] K. Hu, D. Wang, M. Zhou, J. H. Bae, Y. Yu, H. Xin, and M. V. Mirkin, Anal. Chem. **91**, 12935 (2019).
[16] S. Shchanikov, A. Zuev, I. Bordanov, S. Danilin, V. Lukoyanov, D. Korolev, A. Belov, Y. Pigareva, A. Gladkov, A. Pimashkin *et al.*, Chaos Solitons Fractals **142**, 110504 (2021).
[17] A. Noy and S. B. Darling, Science **379**, 143 (2023).
[18] C. Li, T. Xiong, P. Yu, J. Fei, and L. Mao, ACS Appl. Bio Mater. **4**, 71 (2020).
[19] L. Jubin, A. Poggioli, A. Siria, and L. Bocquet, Proc. Natl. Acad. Sci. U.S.A. **115**, 4063 (2018).
[20] X. Hou, W. Guo, and L. Jiang, Chem. Soc. Rev. **40**, 2385 (2011).
[21] S. Ghosal, J. D. Sherwood, and H.-C. Chang, Biomicrofluidics **13**, 011301 (2019).

[22] S. N. Bush, T. T. Volta, and C. R. Martin, Nanomater. Nanotechnol. **10**, 571 (2020).
[23] J. Liu, M. Kvetny, J. Feng, D. Wang, B. Wu, W. Brown, and G. Wang, Langmuir **28**, 1588 (2012).
[24] C. Wei, A. J. Bard, and S. W. Feldberg, Anal. Chem. **69**, 4627 (1997).
[25] W. Q. Boon, T. E. Veenstra, M. Dijkstra, and R. van Roij, Phys. Fluids **34**, 101701 (2022).
[26] H. S. White and A. Bund, Langmuir **24**, 2212 (2008).
[27] L.-J. Cheng and L. J. Guo, Nano Lett. **7**, 3165 (2007).
[28] Z. S. Siwy, Adv. Funct. Mater. **16**, 735 (2006).
[29] Z. Siwy, Y. Gu, H. Spohr, D. Baur, A. Wolf-Reber, R. Spohr, P. Apel, and Y. Korchev, Europhys. Lett. **60**, 349 (2002).
[30] A. Fuliński, I. Kosińska, and Z. Siwy, New J. Phys. **7**, 132 (2005).
[31] Z. Siwy, I. D. Kosińska, A. Fuliński, and C. R. Martin, Phys. Rev. Lett. **94**, 048102 (2005).
[32] D. Duleba, P. Dutta, S. Denuga, and R. P. Johnson, ACS Meas. Sci. **2**, 271 (2022).
[33] W.-J. Lan, M. A. Edwards, L. Luo, R. T. Perera, X. Wu, C. R. Martin, and H. S. White, Acc. Chem. Res. **49**, 2605 (2016).
[34] I. Vlassiouk, S. Smirnov, and Z. Siwy, ACS Nano **2**, 1589 (2008).
[35] C. Kubeil and A. Bund, J. Phys. Chem. C **115**, 7866 (2011).
[36] S. Dal Cengio and I. Pagonabarraga, J. Chem. Phys. **151**, 044707 (2019).
[37] A. R. Poggioli, A. Siria, and L. Bocquet, J. Phys. Chem. B **123**, 1171 (2019).
[38] Y. Uematsu, Phys. Fluids **34**, 122012 (2022).
[39] M. L. Kovarik, K. Zhou, and S. C. Jacobson, J. Phys. Chem. B **113**, 15960 (2009).
[40] C.-Y. Lin, L.-H. Yeh, and Z. S. Siwy, J. Phys. Chem. Lett. **9**, 393 (2018).
[41] Z. Siwy, P. Apel, D. Baur, D. D. Dobrev, Y. E. Korchev, R. Neumann, R. Spohr, C. Trautmann, and K.-O. Voss, Surf. Sci. **532**, 1061 (2003).
[42] Z. Siwy and A. Fuliński, Phys. Rev. Lett. **89**, 198103 (2002).
[43] D. Wang, M. Kvetny, J. Liu, W. Brown, Y. Li, and G. Wang, J. Am. Chem. Soc. **134**, 3651 (2012).
[44] Y. Li, D. Wang, M. M. Kvetny, W. Brown, J. Liu, and G. Wang, Chem. Sci. **6**, 588 (2015).
[45] D. Wang, J. Liu, M. Kvetny, Y. Li, W. Brown, and G. Wang, Chem. Sci. **5**, 1827 (2014).
[46] D. Wang and G. Wang, J. Electroanal. Chem. **779**, 39 (2016).
[47] D. Wang, W. Brown, Y. Li, M. Kvetny, J. Liu, and G. Wang, Anal. Chem. **89**, 11811 (2017).
[48] Q. Sheng, Y. Xie, J. Li, X. Wang, and J. Xue, Chem. Commun. (Cambridge) **53**, 6125 (2017).
[49] W. Brown, Y. Li, R. Yang, D. Wang, M. Kvetny, H. Zheng, and G. Wang, Chem. Sci. **11**, 5950 (2020).
[50] W. Brown, M. Kvetny, R. Yang, and G. Wang, J. Phys. Chem. C **126**, 10872 (2022).
[51] W. Brown, M. Kvetny, R. Yang, and G. Wang, J. Phys. Chem. C **125**, 3269 (2021).
[52] D. Wang, W. Brown, Y. Li, M. Kvetny, J. Liu, and G. Wang, Chem. Electro. Chem. **5**, 3089 (2018).
[53] P. Ramirez, J. J. Perez-Grau, J. Cervera, S. Nasir, M. Ali, W. Ensinger, and S. Mafe, Appl. Phys. Lett. **118**, 181903 (2021).
[54] L. Chua, IEEE Trans. Circuit Theory **18**, 507 (1971).
[55] D. B. Strukov, G. S. Snider, D. R. Stewart, and R. S. Williams, Nature (London) **453**, 80 (2008).
[56] L. Chua, Semicond. Sci. Technol. **29**, 104001 (2014).
[57] F. Caravelli and J. P. Carbajal, Technologies de l'Information et Societe **6**, 118 (2018).
[58] L. Chua, Nanotechnology **24**, 383001 (2013).
[59] Y. van De Burgt, A. Melianas, S. T. Keene, G. Malliaras, and A. Salleo, National electronics review **1**, 386 (2018).
[60] S. T. Keene, P. Gkoupidenis, and Y. Van de Burgt, in *Organic Flexible Electronics* (Elsevier, New York, 2021), pp. 531–574, 10.1016/B978-0-12-818890-3.00018-7.
[61] E. Chicca and G. Indiveri, Appl. Phys. Lett. **116**, 120501 (2020).
[62] D. V. Christensen, R. Dittmann, B. Linares-Barranco, A. Sebastian, M. Le Gallo, A. Redaelli, S. Slesazeck, T. Mikolajick, S. Spiga, S. Menzel *et al.*, Neuromorphic Comput. Eng. **2**, 022501 (2022).
[63] M. P. Sah, H. Kim, and L. O. Chua, IEEE Circuits Syst. Mag. **14**, 12 (2014).
[64] C. D. Schuman, T. E. Potok, R. M. Patton, J. D. Birdwell, M. E. Dean, G. S. Rose, and J. S. Plank, arXiv:1705.06963.
[65] T. Venkatesan and S. Williams, Appl. Phys. Rev. **9**, 010401 (2022).
[66] J. Zhu, T. Zhang, Y. Yang, and R. Huang, Appl. Phys. Rev. **7**, 011312 (2020).
[67] A. Mehonic and A. J. Kenyon, Nature (London) **604**, 255 (2022).
[68] V. K. Sangwan and M. C. Hersam, Nat. Nanotechnol. **15**, 517 (2020).
[69] F. Caravelli, F. C. Sheldon, and F. L. Traversa, Sci. Adv. **7**, eabh1542 (2021).
[70] S. T. Keene, C. Lubrano, S. Kazemzadeh, A. Melianas, Y. Tuchman, G. Polino, P. Scognamiglio, L. Cinà, A. Salleo, Y. van de Burgt *et al.*, Nat. Mater. **19**, 969 (2020).
[71] P. C. Harikesh, C.-Y. Yang, D. Tu, J. Y. Gerasimov, A. M. Dar, A. Armada-Moreira, M. Massetti, R. Kroon, D. Bliman, R. Olsson *et al.*, Nat. Commun. **13**, 1 (2022).
[72] I. Krauhausen, D. A. Koutsouras, A. Melianas, S. T. Keene, K. Lieberth, H. Ledanseur, R. Sheelamanthula, A. Giovannitti, F. Torricelli, I. Mcculloch *et al.*, Sci. Adv. **7**, eabl5068 (2021).
[73] P. D. Marasco, J. S. Hebert, J. W. Sensinger, D. T. Beckler, Z. C. Thumser, A. W. Shehata, H. E. Williams, and K. R. Wilson, Sci. Rob. **6**, eabf3368 (2021).
[74] L. Yuan, S. Liu, W. Chen, F. Fan, and G. Liu, Adv. Electron. Mater. **7**, 2100432 (2021).
[75] L. Squire, D. Berg, F. Bloom, S. du Lac, A. Ghosh, and N. Spitzer, *Fundamental Neuroscience*, 3rd ed. (Academic Press, New York, 2008), Chap. 11.
[76] B. P. Bean, Nat. Rev. Neurosci. **8**, 451 (2007).
[77] T. Xiong, C. Li, X. He, B. Xie, J. Zong, Y. Jiang, W. Ma, F. Wu, J. Fei, P. Yu *et al.*, Science **379**, 156 (2023).

[78] P. Robin, T. Emmerich, A. Ismail, A. Niguès, Y. You, G.-H. Nam, A. Keerthi, A. Siria, A. Geim, B. Radha *et al.*, Science **379**, 161 (2023).

[79] B. Xie, T. Xiong, W. Li, T. Gao, J. Zong, Y. Liu, and P. Yu, Chemistry Asian J. **17**, e202200682 (2022).

[80] D. Kim and J.-S. Lee, ACS Appl. Electr. Mater. **5**, 664 (2023).

[81] K. Lucas, J. Physiol. **38**, 113 (1909).

[82] L. Squire, D. Berg, F. Bloom, S. du Lac, A. Ghosh, and N. Spitzer, Fundamental Neuroscience (Ref. [75]), Chap. 6.

[83] G. S. Cymbalyuk, Q. Gaudry, M. A. Masino, and R. L. Calabrese, J. Neurosci. **22**, 10580 (2002).

[84] E. Marder and V. Thirumalai, Neural Netw. **15**, 479 (2002).

[85] S. M. Sherman, Trends Neurosci. **24**, 122 (2001).

[86] P. Robin, N. Kavokine, and L. Bocquet, Science **373**, 687 (2021).

[87] B. J. Kirby and E. F. Hasselbrink, Jr., Electrophoresis **25**, 187 (2004).

[88] M. Aarts, W. Q. Boon, B. Cuénod, M. Dijkstra, R. van Roij, and E. Alarcon-Llado, ACS Appl. Mater. Interfaces (2022).

[89] See Supplemental Material at http://link.aps.org/supplemental/10.1103/PhysRevLett.130.268401 for the derivation of Eq. (6), a discussion of the range of validity of the analytical approximation, and an analysis of the circuit as a dynamical system, which includes Refs. [90–96].

[90] R. FitzHugh, Biophys. J. **1**, 445 (1961).

[91] J. Nagumo, S. Arimoto, and S. Yoshizawa, Proc. IRE **50**, 2061 (1962).

[92] J. Bisquert, J. Phys. Chem. Lett. **12**, 11005 (2021).

[93] W. C. Troy, J. Math. Anal. Appl. **54**, 678 (1976).

[94] A. Rabinovitch and I. Rogachevskii, Chaos **9**, 880 (1999).

[95] J. K. Hale and H. Koçak, *Dynamics and Bifurcations* (Springer Science & Business Media, New York, 2012), Vol. 3, Chap. 11.

[96] S. Lynch, *Dynamical Systems with Applications using* MATLAB (Springer, New York, 2004), Chap. 13.

[97] V. S. Markin, A. G. Volkov, and L. Chua, Plant Signaling Behav. **9**, e972887 (2014).

[98] C. Multiphysics, Introduction to COMSOL Multiphysics Version: 5.4 (1998), https://doc.comsol.com/5.4/doc/com.comsol.help.comsol/IntroductionToCOMSOLMultiphysics.pdf.

[99] R. W. Pryor, *Multiphysics Modeling using* COMSOL®*: A First Principles Approach* (Jones & Bartlett Publishers, Sudbury, 2009).

[100] A. L. Hodgkin and A. F. Huxley, J. Physiol. **117**, 500 (1952).

[101] W. Rall, Compr. Physiol. 39 (2011).

[102] R. FitzHugh, J. Theor. Biol. **40**, 517 (1973).

[103] W. Rall, Ann. N.Y. Acad. Sci. **96**, 1071 (1962).

[104] J. A. Halter and J. Clark, Jr., J. Theor. Biol. **148**, 345 (1991).

[105] E. Hay, S. Hill, F. Schürmann, H. Markram, and I. Segev, PLoS Comput. Biol. **7**, e1002107 (2011).

[106] M. L. Hines and N. T. Carnevale, Neural Comput. **9**, 1179 (1997).

[107] M. H. Kole, S. U. Ilschner, B. M. Kampa, S. R. Williams, P. C. Ruben, and G. J. Stuart, Nat. Neurosci. **11**, 178 (2008).

[108] L. J. Gentet, G. J. Stuart, and J. D. Clements, Biophys. J. **79**, 314 (2000).